MIMO Antennas for a Terrestrial Point-to-Point Wireless Link: From the Optimum Antenna Spacing to a Compact Array

Xuan Hui Wu[1, *], Douglas Smith[2], and Thomas Yang[3]

Abstract—Multiple-input-multiple-output antennas are investigated for terrestrial point-to-point wireless link. The lack of rich scatters in a terrestrial wireless channel results in an ill-conditioned channel matrix for a long range link with compact arrays, which can cause a high bit error rate. This paper demonstrates that the channel matrix can be improved by carefully selecting the antenna spacing. Unfortunately, an optimum antenna spacing that guarantees a good channel matrix is too large to implement for most long range terrestrial wireless links. On the other hand, a channel capacity study of an 8×8 link reveals that multiple antennas do provide more capacity even with small antenna spacing. Constellation multiplexing is then applied to the compact array configuration to solve the unreliable communication problem. In addition, a multilevel maximum ratio combining technique is introduced to improve detection efficiency.

1. INTRODUCTION

Multiple-input-multiple-output (MIMO) antenna technology has been proven to tremendously increase wireless communication systems' capacity without extra frequency bandwidth [1–4]. It relies on rich scatters in the wave propagation environment to construct virtually independent sub-channels. For a MIMO link, the received signals are

$$\mathbf{s_r} = \mathbf{H s_t} + \mathbf{n} \tag{1}$$

where $\mathbf{s_t}$ is the transmit signal vector, $\mathbf{s_r}$ the received signal vector, $\mathbf{H}$ the channel matrix, and $\mathbf{n}$ the noise vector. In a rich scattering environment such as urban areas, the channel matrix is well conditioned and the transmitted data can be recovered as

$$\mathbf{s'_t} = \mathbf{H}^{-1}\mathbf{s_r} \tag{2}$$

The idea of using multiple antennas to increase data is also introduced to terrestrial microwave links [5, 6]. However, for a terrestrial point-to-point wireless link as shown in Fig. 1(a), the channel is dominated by line-of-sight paths and possibly additional ground reflection paths. The lack of scatters in such a channel may result in a ill-conditioned channel matrix, and the computation of (2) becomes unreliable. Repeaters can be used to improve the condition of the channel matrix, but it requires expensive upgrade of the infrastructure [7]. At millimeter wave frequency, MIMO technology is implemented for a line-of-sight short distance communication [8–10]. Optimal antenna array design is discussed in [11] and adaptive strategy of multiplexing and beamforming is presented in [12] for line-of-sight MIMO systems.
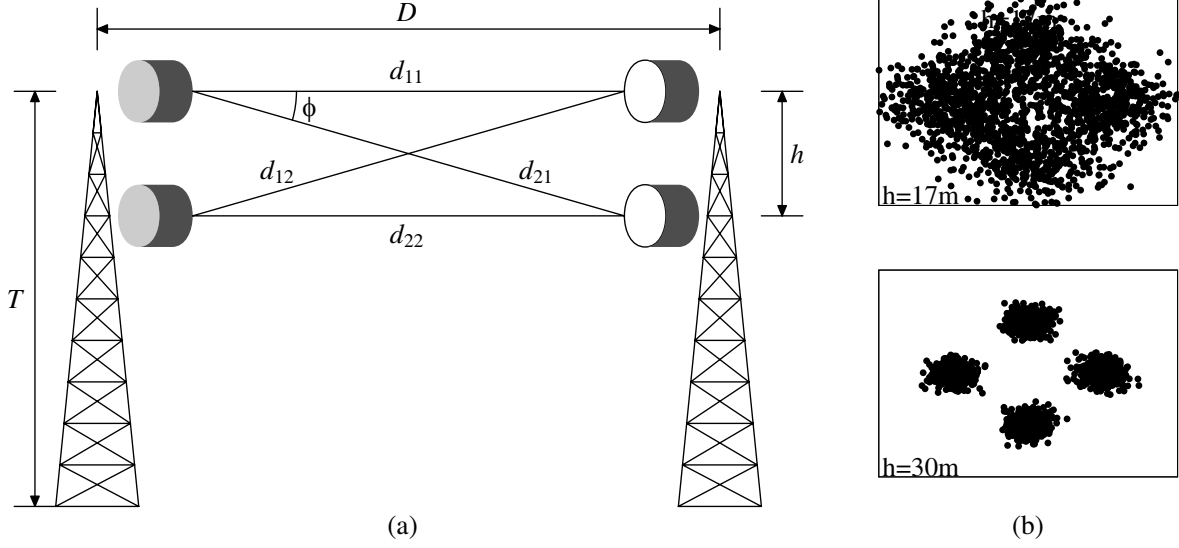
Without scatters, a proper arrangement of antennas' positions may produce a well behaved channel matrix. A 2×2 terrestrial MIMO link is shown in Fig. 1(a), with tower height $T = 50\,\mathrm{m}$, tower to tower

Figure 1. (a) A 2×2 terrestrial MIMO link and (b) the received constellation diagram with $T = 50\,\text{m}$, $D = 50\,\text{km}$, $850\,\text{MHz}$ carrier, $\text{SNR} = 30\,\text{dB}$ and different antenna spacing values.

distance $D = 50\,\text{km}$, carrier frequency of $850\,\text{MHz}$, $30\,\text{dB}$ signal to noise ratio (SNR) and a quadrature phase shift key (QPSK) modulation scheme. Figs. 1(b) and (c) show the received constellation diagrams for different antenna spacing if (2) is applied. Clearly, in order to achieve a low bit error rate (BER), a spacing of $30\,\text{m}$ is required for this example, which is impractical.

This paper investigates the performance of a terrestrial point-to-point MIMO link. Our study is carried out by exploring the channel condition number, eigenvalue distribution, channel capacity and the BER performance of a communication link. The channel model incorporates wave propagation phenomena such as ground reflection and polarization mismatch. In Section 2, the effects of antenna spacing on the condition number and eigenvalue of the channel matrix and BER performance are studied. Both long range and short range links are discussed. Section 3 presents an 8×8 MIMO link. It is implemented by deploying four dual-polarized antennas at both the transmitting and receiving sides. The condition when the ground reflection should be considered is discussed. The channel matrix is derived using a two-path model, and polarization mismatch is incorporated in the model. The condition number of the channel matrix and the capacity of the channel is examined. Section 4 presents a constellation multiplexing technique to solve the unreliable communications when compact antenna arrays are deployed [13]. Excellent BER performance is observed. Section 5 presents a multilevel maximum ratio combining algorithm to improve detection efficiency. Section 6 draws the conclusions.

2. ANTENNA SPACING EFFECTS FOR A 2×2 LINK

For the 2×2 MIMO link shown in Fig. 1(a), the channel matrix can be computed as

$$\mathbf{H} = \begin{bmatrix} \exp(-jkd_{11}) & \exp(-jkd_{12}) \\ \exp(-jkd_{21}) & \exp(-jkd_{22}) \end{bmatrix} \tag{3}$$

where k is the wave number. As discussed before, without rich scatters, and the channel matrix may be ill conditioned and will produce poor constellation diagram at the receiver. Specially, if the tower to tower distance is infinite while the antenna spacing is finite, all signal paths are parallel to each other and have the same length, so $d_{11} = d_{12} = d_{21} = d_{22}$. In this case, $\mathbf{H}$ is singular and cannot be inverted as in (2). Alternatively, if the antenna spacing h is carefully chosen such that $d_{12} - d_{11} = d_{21} - d_{22} = \lambda/4$, where λ is the carrier wavelength, the channel matrix can be written as

$$\mathbf{H} = \begin{bmatrix} 1 & -j \\ -j & 1 \end{bmatrix}. \tag{4}$$

This is a well conditioned matrix with condition number 1, and it can be inverted as

$$\mathbf{H}^{-1} = 0.5 \begin{bmatrix} 1 & j \\ j & 1 \end{bmatrix}. \tag{5}$$

Such an h is referred to as the optimum antenna spacing h_{opt}, because it gives the best behaving channel matrix. The h_{opt} can be calculated as

$$h_{\mathrm{opt}} = D \tan(\phi) \tag{6}$$

where D is the tower to tower distance and

$$\phi = \cos^{-1} \frac{D}{D + \lambda/4} \tag{7}$$

is the angle between two different signal paths as shown in Fig. 1(a).

For a wireless link over 30 km, Fig. 2(a) shows the relationship of h_{opt} and tower to tower distance D with different carriers. Obviously, h_{opt} increases with tower to tower distance and decreases with carrier frequency. It can be seen that in order to achieve a practical optimum antenna spacing for a typical communication range, say 50 km, very high carrier frequency is required. Specifically, at 1 GHz, $h_{\mathrm{opt}} = 85$ m, which is impractical. Even at 80 GHz, which is the highest band for terrestrial microwave link, h_{opt} is about 10m, and it is still difficult to realize. The large antenna spacing not only limits the number of antennas that can be installed on towers, but it also introduces additional loss due to extended cables that connect antennas. On the other hand, a short range wireless link at millimeter wave is able to implement its h_{opt}. For example, 60 GHz band is an unlicensed band for a communication range less than 2.5 km. Fig. 2(b) gives the h_{opt} for tower to tower distance from 1 km to 2.5 km at 60 GHz, where the optimum antenna spacing is about 2 m, which is realizable.

Figure 3 shows the condition number and eigenvalue ratio of the 2×2 link where the eigenvalue ratio is defined as the magnitude of the ratio of the small eigenvalue over the large eigenvalue. As seen, two eigenvalues have the same magnitudes at the optimum antenna spacing where the condition number equals 1. If antenna spacing decreases from its optimum value, the condition number of the channel matrix in (3) will increase drastically and the eigenvalue ratio reduces to 0. This results in the computation of (2) being unreliable for a compact array. Monte Carlo simulation is carried out to obtain the BER performance of the MIMO link with different antenna spacing. QPSK is adopted and the transmitted constellation diagram is shown in Fig. 4(a). At the receiving side, (2) is applied first to recover the transmitted signal. Then, the detection is carried out based on the location of the recovered signal in the constellation plane. As shown in Fig. 4(a), two 45° lines divide the receiving constellation plane into four regions D_A, D_B, D_C and D_D. If the recovered signal obtained from (2) falls into region D_n with n representing A, B, C, or D, then S_n in the transmitted constellation diagram is detected as
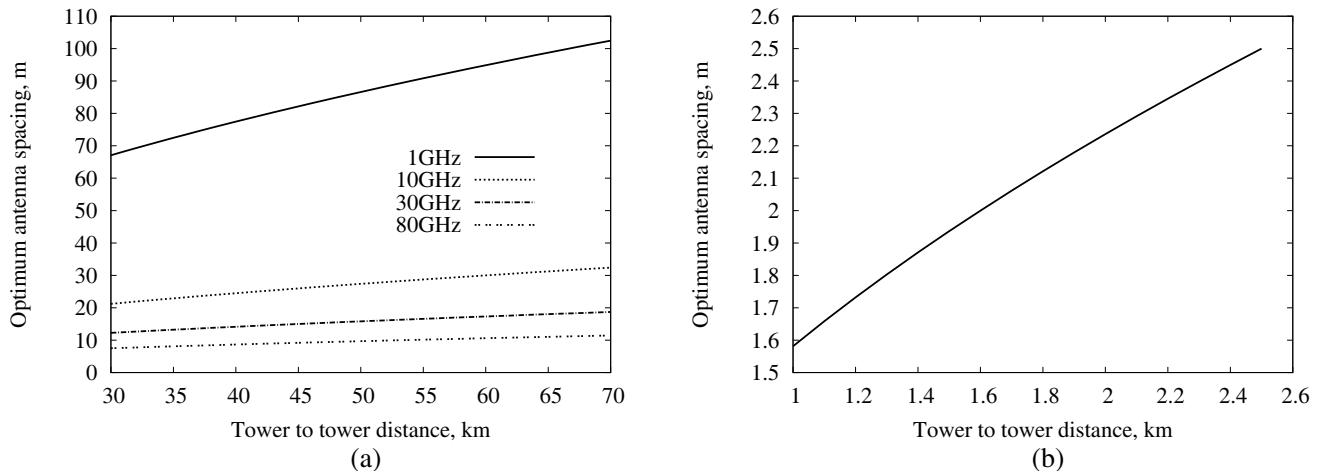
Figure 2. Optimum antenna spacing h_{opt} for a (a) long range link and (b) a 60 GHz short range link.
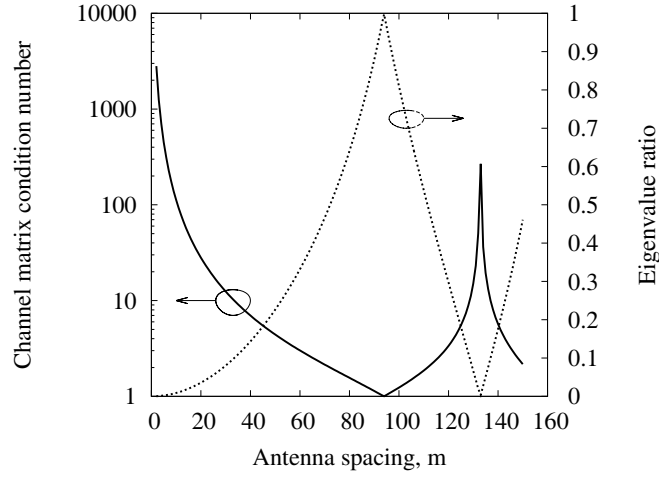
Figure 3. Condition number and eigenvalue ratio of the 2×2 MIMO link, $D = 50\,\mathrm{km}$ and $850\,\mathrm{MHz}$ carrier.
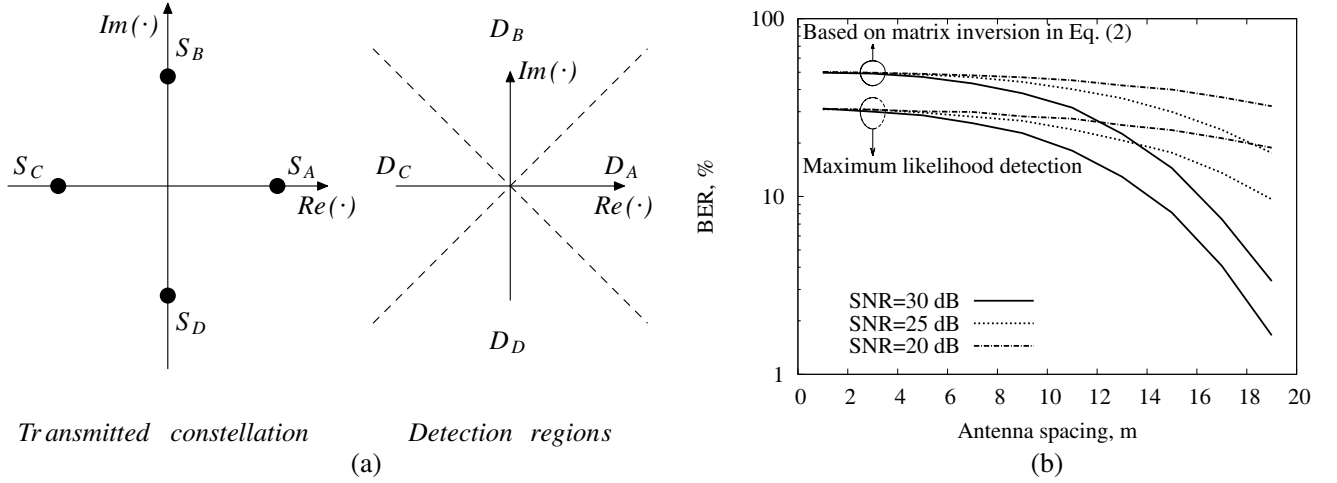
Figure 4. (a) QPSK constellation diagram and the detection regions at the receiver and (b) the resulting BER vs. antenna spacing for the 2×2 MIMO link, $D = 50\,\mathrm{km}$ and $850\,\mathrm{MHz}$ carrier.

the transmitted signal. The BER performance vs. antenna spacing using the aforementioned detection scheme is plotted and compared to the maximum likelihood detection in Fig. 4(b). It can be seen that the increased SNR does not improve the BER performance when antenna spacing is small. The receiver based on (2) behaves as a random guess that gives a 50% bit error rate and the maximum likelihood detector also gives a high BER of 30%.

3. AN 8×8 TERRESTRIAL MIMO LINK USING DUAL POLARIZED ANTENNAS

An 8×8 link is studied here. The array configuration is similar to that shown in Fig. 1(a) except that four dual-polarized antennas, either linearly or circularly polarized, are installed on each tower. As mentioned before, a terrestrial wireless link is dominated by a line-of-sight path and a ground reflection path. The signal strength of the reflected path is determined by the antenna position, the antenna gain and the reflection coefficient of the ground. Fig. 5(a) shows a pair of antennas, where the transmitting and receiving antennas are at height of H_t and H_r, respectively. The tilting angle of the reflected signal

path can be obtained as

$$\theta = \tan^{-1}\left(\frac{H_t + H_r}{D}\right). \tag{8}$$

The transmitting antenna points to the center of the receiving array. Assuming the main beam direction of the transmitting antenna is parallel to the ground, if the signal power incident on ground is more than half of that in the main beam direction such that

$$\Theta_{3\,\mathrm{dB}} \geq 2\theta \tag{9}$$

where $\Theta_{3\,\mathrm{dB}}$ is the antenna's half power beam width. The ground reflection is significant, and the reflected path cannot be neglected. Assuming identical half power beam width in the two principal planes, Equation (9) requires an antenna whose gain G satisfies

$$G = \frac{4\pi}{\Theta_{3\,\mathrm{dB}}^2} \leq \frac{\pi}{\theta^2} \tag{10}$$

where θ is given in Equation (8) [14]. Therefore, an antenna with gain less than π/θ^2 will give substantial ground reflection.
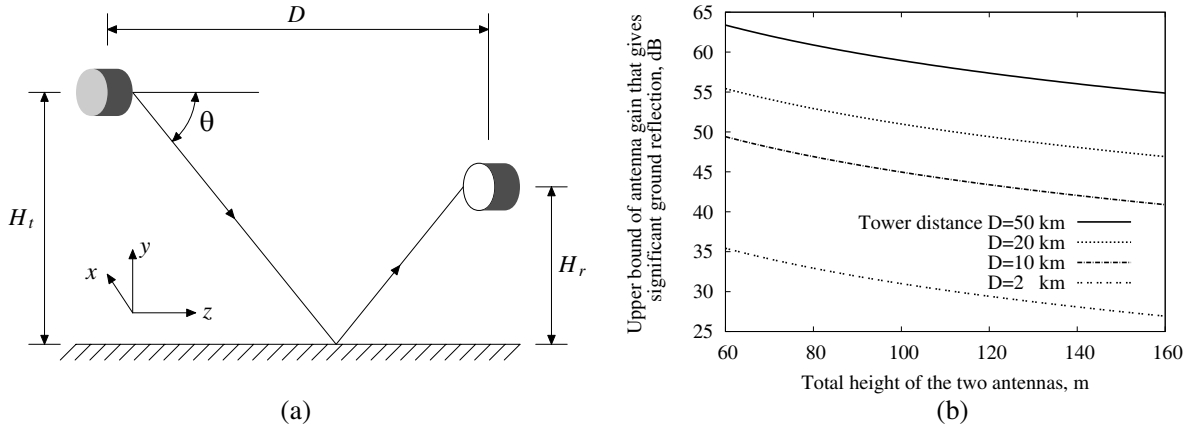
Figure 5. Ground reflection effect. (a) Reflection model and (b) upper bound of antenna gain that gives significant ground reflection, with $G = \pi/\theta^2$ in Equation (10).

If the equality sign is chosen, Equation (10) gives an upper bound for the antenna gain that will cause substantial ground reflection. Fig. 5(b) shows such bound for antenna gain vs. antennas' total height for different antenna spacing. Particularly, given an antenna spacing D and total antenna height $H_t + H_r$, an antenna whose gain below the value in Fig. 5(b) will result in a significant ground reflection. Considering that the maximum gain of most available terrestrial microwave antennas varies between 30 dB to 35 dB for different bands, a long range link with $D \geq 10$ km and a typical tower height of around 50 m will have a strong ground reflection. For a short range like 2 km, the ground reflection may be ignored if the antennas are installed high enough above the ground.

In order to incorporate the ground reflection effect, a two path model is applied when deriving the channel matrix. The elements of the channel matrix can be obtained by tracing the direct and reflected signal paths between each transmitting/receiving antenna pair as

$$a = a_{\mathrm{dir}} + a_{\mathrm{ref}}. \tag{11}$$

where a_{dir} is the channel response due to the direct path. For the antenna configuration in Fig. 5(a), a_{dir} can be calculated based on the Friis transmission equation [14] as

$$a_{\mathrm{dir}} = \sqrt{G_{\mathrm{t,dir}}G_{\mathrm{r,dir}}}\frac{\exp\left[-jk\sqrt{D^2 + (H_t - H_r)^2}\right]}{\sqrt{D^2 + (H_t - H_r)^2}}\hat{\rho}_t \cdot \hat{\rho}_r \tag{12}$$

Table 1. Unit polarization vectors.

	V-pol	H-pol	LHCP	RHCP
Transmitting	$\hat{y}$	$\hat{x}$	$(\hat{y} - j\hat{x})/\sqrt{2}$	$(\hat{y} + j\hat{x})/\sqrt{2}$
Receiving	$\hat{y}$	$\hat{x}$	$(\hat{y} + j\hat{x})/\sqrt{2}$	$(\hat{y} - j\hat{x})/\sqrt{2}$

where $G_{\text{t,dir}}$ and $G_{\text{r,dir}}$ are the transmitting and receiving antenna gain in the direct path direction and $\hat{\rho}_t$ as well as $\hat{\rho}_r$ are the unit polarization vectors of the transmitting and receiving antennas, respectively. $\hat{\rho}_t$ and $\hat{\rho}_r$ are listed in Table 1, where $\hat{x}$ is parallel and $\hat{y}$ is perpendicular to the ground as illustrated in Fig. 5(a).

Similarly, a_{ref} in (11) is the channel response due to the reflected path and can be calculated as

$$a_{\text{ref}} = \sqrt{G_{\text{t,ref}}G_{\text{r,ref}}} \frac{\exp\left[-jk\sqrt{D^2 + (H_t + H_r)^2}\right]}{\sqrt{D^2 + (H_t + H_r)^2}}$$
$$\times \left[(\hat{\rho}_t \cdot \hat{x}\Gamma_h)\hat{x} + (\hat{\rho}_t \cdot \hat{y}\Gamma_v)\hat{y}\right] \cdot \hat{\rho}_r \tag{13}$$

where $G_{\text{t,ref}}$ and $G_{\text{r,ref}}$ are the transmitting and receiving antenna gains in the reflected path direction, and Γ_h and Γ_v are the ground reflection coefficients for horizontally and vertically polarized waves, respectively [14]. If the ground is modeled as a semi-infinite dielectric material with a relative permittivity ϵ_r, the reflection coefficients can be calculated as

$$\Gamma_h = \frac{\sqrt{\epsilon_r}\cos\theta_t - \cos\theta_i}{\sqrt{\epsilon_r}\cos\theta_t + \cos\theta_i} \tag{14}$$

$$\Gamma_v = \frac{\sqrt{\epsilon_r}\cos\theta_i - \cos\theta_t}{\sqrt{\epsilon_r}\cos\theta_i + \cos\theta_t} \tag{15}$$

where θ_i and θ_t are the incident and transmission angles whose relationship is determined by the Snell's Law [15]. Different types of ground result in different ϵ_r values. In this study, the averaged value of 15 is used.

With Equations (11)–(15), the 8×8 channel matrix can be constructed. With the same tower to tower distance and carrier frequency as in Fig. 3, the condition numbers are plotted and compared to the 2×2 link in Fig. 6(a). The h_{opt} of the 8×8 link is reduced to a value of around 65 m, but grows drastically when the antenna spacing decreases from its optimum value. The eigenvalue distribution of the 8×8 link are plotted in Fig. 6(b) and Fig. 6(c), for the link without and with ground reflection, respectively. Given an antenna spacing, the resulting eigenvalues are normalized by the maximum value. Without ground reflection, the channel responses for the two orthogonal polarization waves are the same and so give identical eigenvalues. So, each curve in Fig. 6(b) is actually two overlapped curves. However, with ground reflection, the channel response depends on wave polarization because the ground reflection coefficient is polarization dependent. So, there are eight distinct curves in Fig. 6(c). As shown, for a compact array with small antenna spacing, there are only two eigenvalues with nontrivial values, which means only two instead of eight parallel channels can be constructed. The plots of the 8×8 links in Fig. 6 are polarization independent. Therefore, if only two orthogonal polarizations, either linear or circular, are utilized for each antenna, the condition number and eigenvalue distributions of the 8×8 channel matrix remain the same.

On the other hand, the analysis of the channel capacity reveals that increasing the number of antennas does improve the channel capacity as shown in Fig. 7. Similar to Fig. 6, the result of the 8×8 link is polarization independent if two orthogonal polarizations are used for each antenna. The channel capacity is computed as

$$C = \log_2\left[\det\left(I_{N_r} + \frac{\text{SNR}}{N_t}HH^T\right)\right] \tag{16}$$

where $\det(\cdot)$ is the determinant of a square matrix, $(\cdot)^H$ the conjugate transpose of a matrix, I_{N_r} a unit matrix whose dimension equals to the number of receiving antenna ports N_r, and N_t the number
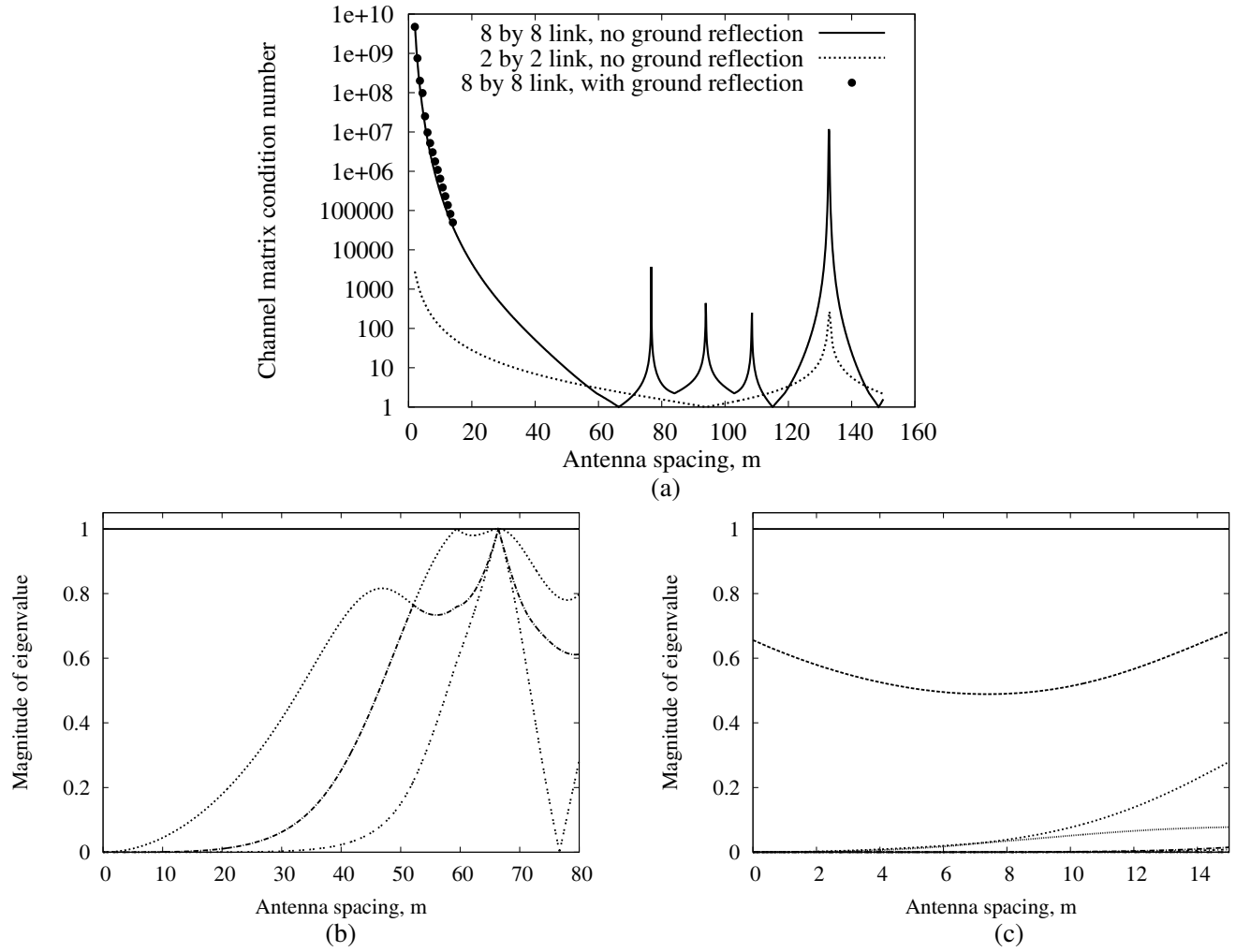
Figure 6. (a) Condition number comparison, (b) eigenvalue distribution of the 8×8 link without ground reflection and (c) including ground reflection, with $D = 50 \, \text{km}$ and $850 \, \text{MHz}$ carrier.

of transmitting antenna ports [2]. Specifically, the channel capacity increases with the number of antennas even with small antenna spacing. For nonuniform antenna arrays, the array configuration can be optimized to maximize the channel capacity [16].

4. CONSTELLATION MULTIPLEXING FOR A COMPACT ANTENNA ARRAY

With sufficient scatters, the channel matrix is well conditioned. Isolated sub-channels can be constructed virtually for the transmission of multiple data streams without mutual interference. For a terrestrial wireless link, the lack of scatters makes the sub-channels not isolated. Instead, there is strong coupling between the sub-channels. Therefore, different data streams are mixed together in the channel and becomes difficult to separate at the receiver.

However, the aforementioned difficulty arises only if identical constellation diagrams are applied at all transmitting antennas. If some sort of differences are introduced to the modulation scheme of each transmitting antenna, such differences can be utilized at the receiving side to separate data stream. This leads to a technique called constellation multiplexing [13]. Take the 2×2 link in Fig. 1(a) for example, Fig. 8(a) shows the transmitted and received constellation diagrams of a 2×2 link after applying constellation multiplexing. The two transmitting antennas both apply QPSK but with different magnitude. S_n with $n \in \{1, 2, 3, 4\}$ is transmitted by one antenna. S_p with $p \in \{A, B, C, D\}$ is
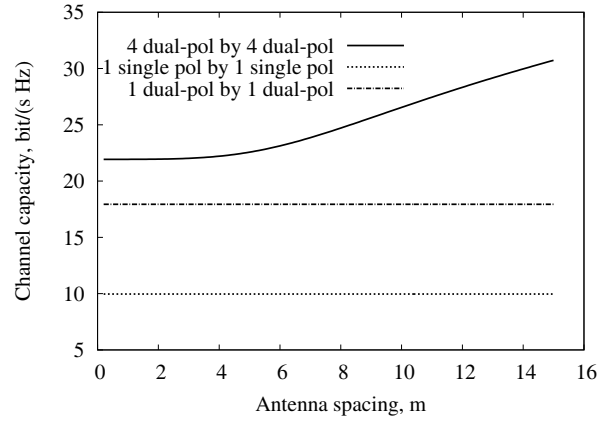
Figure 7. Channel capacity for different array configurations, with $T = 50\,\text{m}$, $D = 50\,\text{km}$, $850\,\text{MHz}$ carrier and $30\,\text{dB}$ SNR.
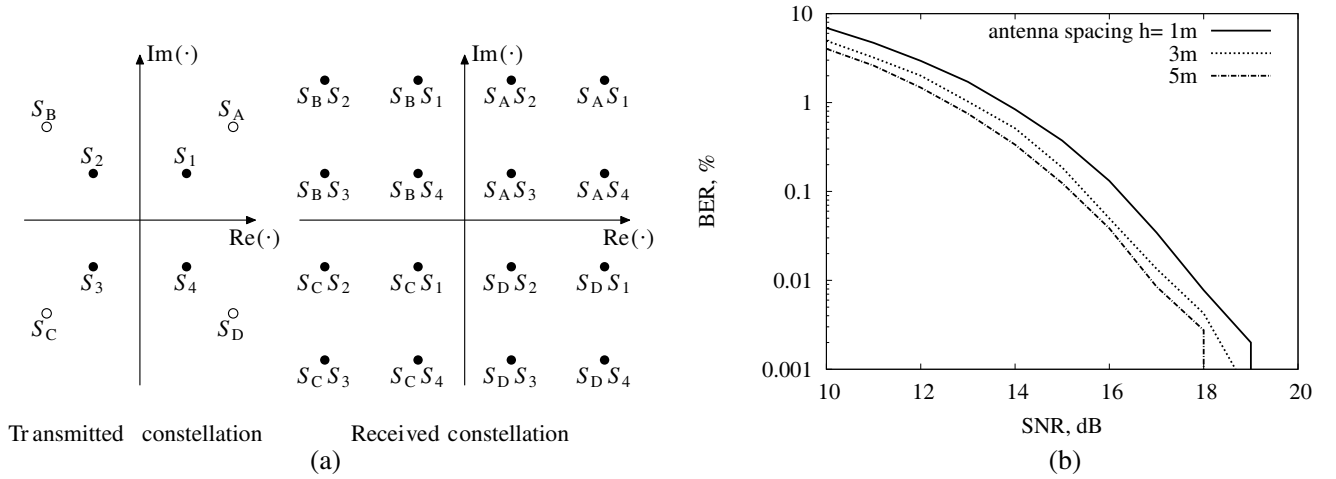
Figure 8. (a) Constellation multiplexing and (b) its BER vs. SNR performance with $T = 50\,\text{m}$, $D = 50\,\text{km}$ and $850\,\text{MHz}$ carrier.
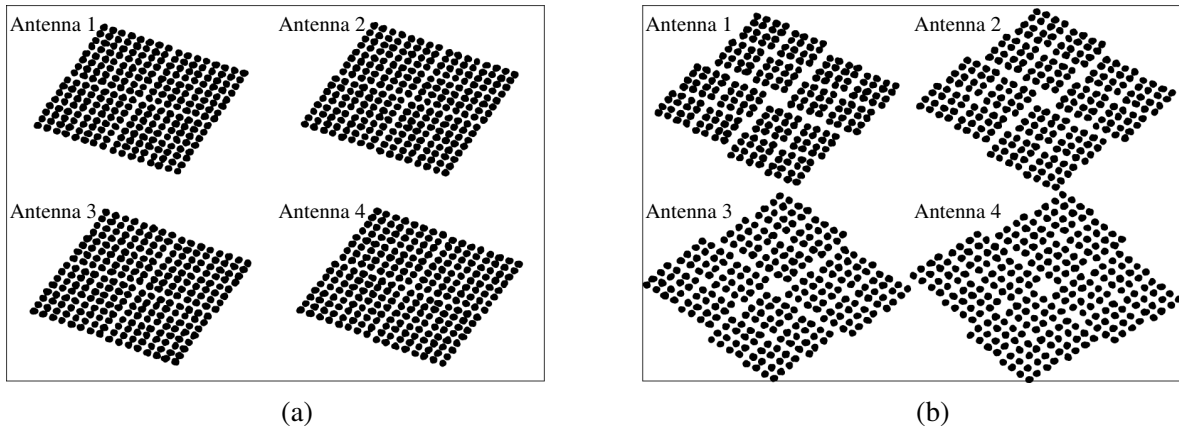
Figure 9. Received constellation diagram with constellation multiplexing, SNR $= 30\,\text{dB}$ and antenna spacing (a) $h = 1\,\text{m}$, (b) $h = 5\,\text{m}$.

transmitted by another antenna. Each receiving antenna receives the superposition of these two sets of QPSK signals, which turns out to be 16 distinct points on the received constellation diagram. Each receiving antenna receives a higher order constellation diagram compared to the transmitting side. As illustrated, the transmitted data can be decoded based on the location of the received signal on the constellation diagram.

An optimum detector referred to as Maximum Likelihood detector can be used to detect S_n and S_p [17, 18]. With the channel matrix $\mathbf{H}$ known at the receiver, the signal received due to the transmission of any combination of S_n and S_p in Fig. 8(a) is known as $\mathbf{Hs_t}$ where $\mathbf{s_t} = [S_n \quad S_p]^T$ in this example. As a result, the transmitted data can be decoded as the pair (S_n, S_p) that gives the minimum difference between the received signal and the signal supposed to receive as

$$\underset{n\in\{1,2,3,4\},p\in\{A,B,C,D\}}{\arg\min} \parallel \mathbf{Hs_t} - \mathbf{s_r} \parallel^2 \tag{17}$$

where $\parallel \cdot \parallel$ gives the Euclidean norm of a vector. The computation of Equation (17) is a searching procedure and does not involve any matrix inversion. The searching dimension of the Maximum Likelihood detector is M^{N_t}, where M is the number of different waveforms transmitted by each antenna and N_t is the number of transmitting antennas. Note that Equation (17) does not require the same number of receiving and transmitting antennas as in Equation (2). One receiving antenna is sufficient to separate the data streams from different transmitters by only using one element of the vector $\mathbf{Hs_t} - \mathbf{s_r}$ in Equation (17). In the case of multiple receiving antennas, incorporation of all received signals will make the detector more robust.

Considering the 8×8 link in Section 3, if linear polarization is used, the link can be considered as two isolated 4×4 links, one for each polarization. This is because ground reflection does not introduce coupling of the two linear polarizations, and a good reflector antenna has excellent cross polarization discrimination level of 30dB to 35dB. Hence, a 4×4 link with vertical polarization is studied. Constellation multiplexing of QPSK is applied such that the magnitude of the signals are $2^{m-1}/\sqrt{85}$, where $m \in [1, 2, 3, 4]$ is the antenna index. The Maximum Likelihood detector in Equation (17) is adopted at the receiver. The BER performance is plotted in Fig. 8(b) with different SNR values for different antenna spacings. Clearly, compared to the results in Fig. 4(b), the constellation multiplexing technique gives excellent results and the BER performance remains almost the same for antenna spacing from 1 m to 7 m. With SNR = 30 dB, the received constellation diagrams at different receiving antennas are illustrated in Fig. 9(a) for antenna spacing of 1 m, and in Fig. 9(b) for antenna spacing of 5m. For the 1m spacing case, all the receiving antennas receive almost identical signals because the channel responses for different antennas are very similar. For the 5m spacing case, difference constellation diagrams are received by different receiving antennas due to the decorrelation of the sub-channels. In addition, twisting of the constellation diagram is observed, for example in Fig. 9(b). This is because with the large spacing of the transmitting antennas, the channel responses from different transmitting antennas to any receiving antenna are different. In Fig. 9, all the constellation diagrams are very clean, which results in reliable detection with low BER. The constellation multiplexing technique form high order modulated symbols in the channel instead of at the transmitter. Therefore, the maximum transmitted power is much less than that of a single transmitting antenna that generates the same high order modulated symbols.

5. MULTILEVEL MAXIMUM RATIO COMBINING FOR HORIZONTALLY DISPLACED MIMO ANTENNAS

Although the maximum likelihood detection gives optimum results, it is inefficient because it searches all the possible combination of the transmitted signals. A real time communication link requires a more efficient detection algorithm.

The maximum ratio combining combines all the signals at different receiving antennas before detection. It is traditionally a receiving diversity technique for a single-input-multiple-output (SIMO) system. With small antenna spacing such as $h = 1$ m, the multiple transmitting antennas may be considered as a single hypothetical antenna that transmits high order modulated signals. Thus, an

$N_t \times N_r$ link is approximated as a $1 \times N_r$ link and the received signals can then be combined as

$$s_{\mathrm{mrc}} = \sum_{n=1}^{N_r} s_n h_n^* \tag{18}$$

where s_n is the received signal at the nth receiving antenna and h_n the channel response from the hypothetical antenna to the nth receiving antenna. Detection is based on the combined signal s_{mrc}. Since there are physically N_t transmitters, h_n can be computed as the averaged channel response from different transmitting antennas to the nth receiving antenna following

$$h_n = \frac{1}{N_t} \sum_{m=1}^{N_t} h_{nm} \tag{19}$$

where h_{nm} is the channel response from the mth transmitting antenna to the nth receiving antenna. However, this technique is very sensitive to the horizontal displacement of the antennas. As shown in Fig. 10(a), for a terrestrial wireless link, reflector antennas are installed separately and a perfect alignment cannot be guaranteed. Furthermore, due to the tilting angle of the antenna tower, a horizontal displacement between antenna elements may be unavoidable. Fig. 10(b) shows the BER performance of the 4×4 link after applying the maximum ratio combining in Equations (18) and
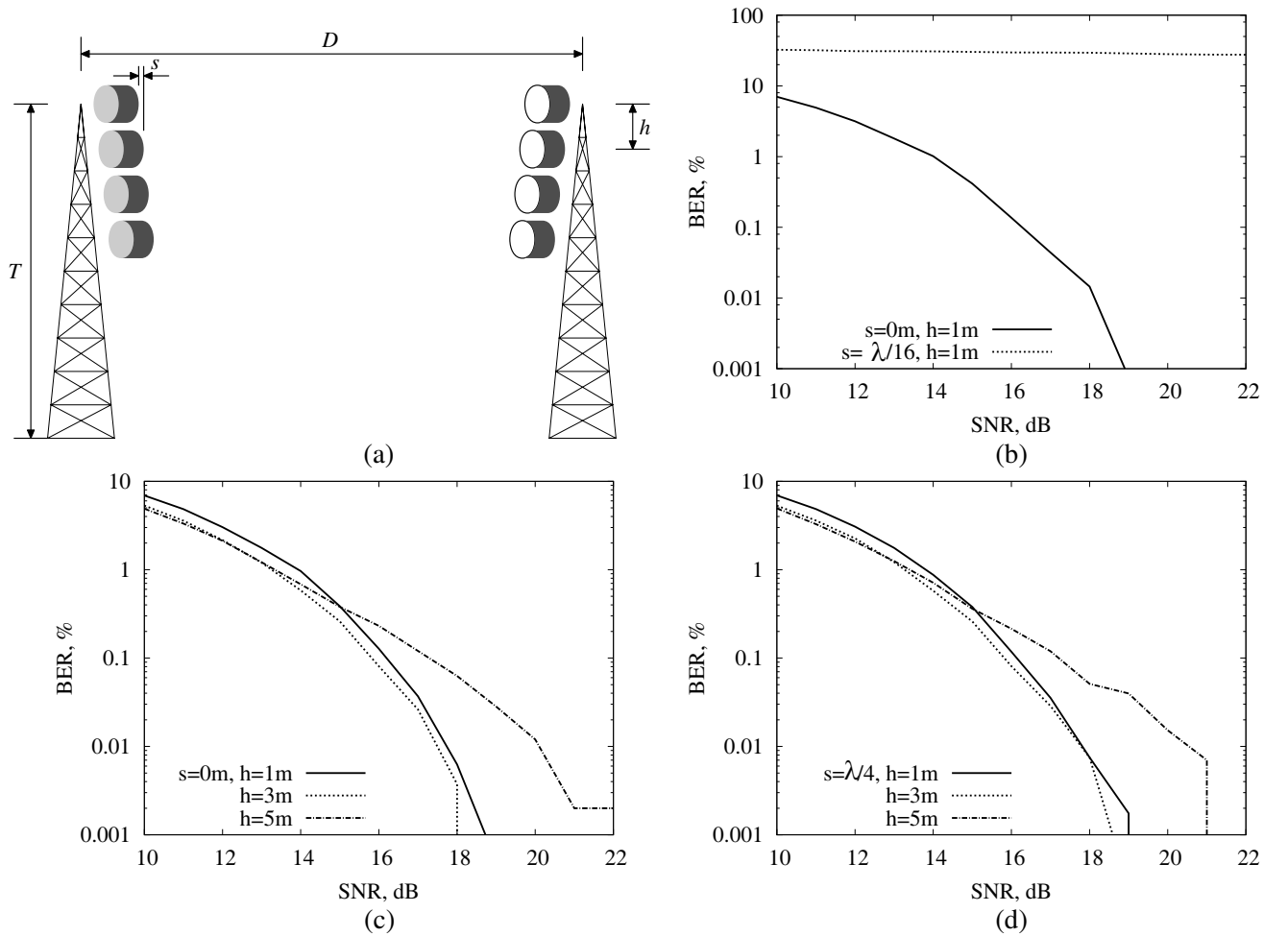
Figure 10. (a) A 4×4 link with displaced MIMO antennas and its BER vs. SNR using (b) maximum ratio combining, (c) multilevel maximum ratio combining for a link without antenna displacement and (d) multilevel maximum ratio combining for a link with antenna displacement $s = \lambda/4$.

(19). Clearly, if the antennas are aligned perfectly without horizontal displacement, the maximum ratio combining performs similar to the maximum likelihood detector shown in Fig. 8(b). However, a slight displacement of $s = \lambda/16$ brings the BER up to around 30%. It is because the maximum ratio combining only compensates the displacement of receiving antennas but not transmitting antennas. The element displacement at the transmitting side also introduces additional phase delay or phase advance of the received signal, which invalidates the hypothetical single transmitting source approximation.

An iterative multilevel maximum ratio combining algorithm solves the aforementioned problem. It detects transmitted signals iteratively from the one with the highest power to the one with the lowest power and adopts different coefficients to combine received signals at different levels. Assuming the transmitted power from the mth antenna is $2^{m-1}/\sqrt{85}$, detection starts from the first transmitting antenna. For the detection of the data from the mth transmitting antenna, the received signals are combined using the channel coefficients from the mth antenna as

$$s_{\mathrm{mmrc},m} = \sum_{n=1}^{N_r} s_n h_{nm}^*. \tag{20}$$

The transmitted data from the mth antenna is then detected based on the phase of $s_{\mathrm{mmrc},m}$. If the transmitted signal from the mth antenna is detected as $s'_{t,m}$, its contribution on all the received signals need to be removed as

$$s_n = s_n - s'_{t,m} h_{nm}, \text{ with } n = 1, \cdots, N_r \tag{21}$$

in order to conduct detection for the $(m + 1)$th transmitting antenna. Equations (20) and (21) are carried out recurrently until all the transmitted data are detected. For the 4×4 link in Fig. 10(a), the BER performance of the multilevel maximum ratio combining is plotted in Fig. 10(c) for $s = 0$ m and in Fig. 10(d) for $s = \lambda/4$, with different antenna spacings. They show almost identical results and the performance is very close to that of the maximum likelihood detection shown in Fig. 8(b).

6. CONCLUSIONS

Multiple-input-multiple-output schemes are investigated for terrestrial point-to-point wireless link. Different from a conventional MIMO link, a terrestrial wireless link is lack of scatters. As a result, the channel matrix is mostly dependent on array configuration parameters, such as antenna spacing, antenna height and tower to tower distance. Antenna spacing effects are studied. For short range communications at millimeter wave frequencies, the optimum antenna spacing that gives a well conditioned channel matrix can be realized. But for long range communications, such optimum spacing is too large to implement. Thus, a practical channel matrix for long range communications is ill conditioned, which gives high BER if the detection relies on channel matrix inversion. An 8×8 MIMO link with four dual-polarized antennas at both transmitting and receiving sides is modeled and studied. The ground reflection and polarization mismatch are incorporated in the channel model. It reveals that although the optimum antenna spacing decreases with more antenna elements, the 8×8 link has worse channel matrix when antenna spacing is small. On the other hand, the channel capacity does increase with more antennas, even with small antenna spacing. The constellation multiplexing technique is then applied to tackle the poor communication reliability problem caused by the ill-conditioned channel matrix. As an example, signals of QPSK with different amplitudes are transmitted by different antennas, and form a high order constellation diagram at the receiver. It is demonstrated that excellent BER performance can be achieved for long range terrestrial MIMO link with compact antenna array using constellation multiplexing. A multilevel maximum ratio combining technique is investigated to improve detection efficiency.

REFERENCES

1. Foschini, G. J., "Layered space-time architecture for wireless communication in a fading environment when using multiple antennas," *Bell Labs. Technical Journal*, Vol. 1, No. 2, 41–59, 1996.

2. Foschini, G. J. and M. J. Gans, "On limits of wireless communications in a fading environment when using multiple antennas," *Wireless Personal Communications*, Vol. 6, No. 3, 311–335, 1998.

3. Gesbert, D., M. Shafi, D. Shiu, P. J. Smith, and A. Naguib, "From theory to practice: An overview of MIMO space-time coded wireless systems," *IEEE J. Slect. Areas Commun.*, Vol. 21, No. 3, 281–302, 2003.

4. Varzakas, P., "Average channel capacity for rayleigh fading spread spectrum MIMO systems," *International Journal of Communication Systems*, Vol. 19, No. 10, 1081–1087, December 2006.

5. Mecklenbrauker, C. F., M. Matthaiou, and M. Viberg, "Eigenbeam transmission over line-of-sight MIMO channels for fixed microwave links," *International ITG Workshop on Smart Antennas*, Apachen, Germany, 24–25 February 2011.

6. Tryggvi, I. and H. Liu, "Line-of-sight MIMO for microwave links: adaptive dual polarized and spatially separated systems," Master of Science Thesis, Chalmers University of Technology, Sweden, July 2009.

7. Walkenhorst, B. T., PhD dissertation, Georgia Institute of Technology, August 2009.

8. Sheldon, C., E. Torkildson, M. Seo, C. P. Yue, U. Madhow, and M. Rodwell, "A 60 GHz line-of-sight 2×2 MIMO link operating at 1.2 Gbps," *Antenna and Propagation Society International Symposium*, San Diego, CA, USA, 5–11 July 2008.

9. Sheldon, C., M. Seo, E. Torkildson, and U. Madhow, "A 2.4 Gb/s millimeter-wave link using adaptive spatial multiplexing," *Antenna and Propagation Society International Symposium*, Toronto, ON, Canada, 11–17 July 2010.

10. Sheldon, C., M. Seo, E. Torkildson, M. Rodwell, and U. Madhow, "Four-channel spatial multiplexing over a millimeter-wave line-of-sight link," *IEEE MTT-S International*, 389–392, Boston, MA, June 7–June 12, 2009.

11. Bøhagen, F., P. Orten, and G. Øien, "Optimal design of uniform rectangular antenna arrays for strong line-of-sight MIMO channels," *EURASIP Journal on Wireless Communications and Networking*, Article ID 45084, 2007.

12. Reggiani, L., B. Baccetti, and L. Dossi, "The role of adaptivity in MIMO line-of-sight systems for high capacity backhauling," *Wireless Personal Communications*, Vol. 74, No. 2, 373–389, January 2014.

13. Gesbert, D. and J. Akhtar, "Transmitting over ill-conditioned MIMO channels: From spatial to constellation multiplexing," *Smart Antennas: State of the Art (Eurasip Book Series on Signal Processing & Communications)*, Hindawi Publishing Corporation, December 2005.

14. Balanis, C. A., *Antenna Theory: Analysis and Design*, 2nd Edition, John Wiley & Sons, Inc., 1996.

15. Pozar, D. M., *Microwave Engineering*, 4th Edition, Wiley, 2011.

16. Recioui, A. and H. Bentarzi, "Capacity optimization of MIMO wireless communication systems using a hybrid genetic-taguchi algorithm," *Wireless Personal Communications*, Vol. 71, No. 2, 1003–1019, July 2013.

17. Jalden, J., "Maximum likelihood detection for the linear MIMO channel," thesis, Royal Institute of Technology, Sweden, 2004.

18. Lomnitz, Y. and D. Andelman, "Efficient maximum likelihood detector for MIMO systems with small number of streams," *Electronics Letters*, Vol. 43, No. 22, October 2007.